Theory of optical excitation spectra and depolarization dynamics in bilayer WS_2 from the viewpoint of excimers

T. Yu and M. W. Wu*

Hefei National Laboratory for Physical Sciences at Microscale and Department of Physics, University of Science and Technology of China, Hefei, Anhui 230026, China

(Received 23 June 2014; revised manuscript received 10 July 2014; published 23 July 2014)

We investigate the optical excitation spectra and the photoluminescence depolarization dynamics in bilayer WS_2. A different understanding of the optical excitation spectra in the recent photoluminescence experiment by Zhu *et al.* (arXiv:1403.6224) in bilayer WS_2 is proposed. In the experiment, four excitations (1.68, 1.93, 1.99, and 2.37 eV) are observed and identified to be the indirect exciton for the Γ valley, trion, A exciton, and B exciton excitations, respectively, with the redshift for the A exciton energy measured to be 30∼50 meV when the sample synthesized from monolayer to bilayer. According to our study, by considering that there exist both the intralayer and charge-transfer excitons in the bilayer WS_2, with interlayer hopping of the hole, there exists an excimer state composed by the superposition of the intralayer and charge-transfer exciton states. Accordingly, we show that the four optical excitations in the bilayer WS_2 are the A charge-transfer exciton, A′ excimer, B′ excimer, and B intralayer exciton states, respectively, with the calculated resonance energies showing good agreement with the experiment. In our picture, the speculated indirect exciton, which involves a high-order phonon absorption/emission process, is not necessary. Furthermore, the binding energy for the excimer state is calculated to be 40 meV, providing reasonable explanation for the experimentally observed energy redshift of the A exciton. Based on the excimer states, we further derive the exchange interaction Hamiltonian. Then the photoluminescence depolarization dynamics due to the electron-hole exchange interaction is studied in the pump-probe setup by the kinetic spin Bloch equations. We find that there is always a residual photoluminescence polarization that is exactly half of the initial one, lasting for an infinitely long time, which is robust against the initial energy broadening and strength of the momentum scattering. This large steady-state photoluminescence polarization indicates that the photoluminescence relaxation time is extremely long in the steady-state photoluminescence experiment, and can be the cause of the anomalously large photoluminescence polarization, nearly 100%, observed in the experiment by Zhu *et al.* in the bilayer WS_2. This steady state is shown to come from the unique form of the exchange interaction Hamiltonian, under which the density matrix evolves into the one which commutes with the exchange interaction Hamiltonian.

DOI: 10.1103/PhysRevB.90.035437 PACS number(s): 71.70.Gm, 71.35.−y, 78.67.−n

I. INTRODUCTION

In the past several years, a new type of two-dimensional material, monolayer (ML) transition-metal dichalcogenides (TMDs), has attracted much attention partly due to its novel optical properties arising from its unique band structures [1–18]. With the direct energy gap and large energy splitting of the valence bands [1–8,13,14], the chiral optical valley selection rule allows the optical control of the valley and spin degrees in ML TMDs, which are mainly realized by excitonic excitation [2,4–6,10–12,19]. Consisting of two ML TMDs, with the added layer degree of freedom, bilayer (BL) TMDs also exhibit rich optical properties due to the preservation of the chiral optical valley selection rule [10,20–28], apart from the new features such as the electrical polarization, electrical-tuned magnetic moments, and magnetoelectric effect [20–23]. Specifically, due to the added layer degree of freedom in BL TMDs, the optical-excited electron and hole can not only stay in the same layer, which forms the intralayer (IL) exciton, but also in different layers referred to as the charge-transfer (CT) exciton [the configurations for the A and B IL (CT) excitons in the K valley are shown in Fig. 1]. Furthermore, due to the interlayer coupling, the two kinds of excitons can couple to form a new elementary excitation: the excimer [29,30]. Therefore, BL TMDs may provide an ideal platform to study the excimer optical excitation and related photoluminescence (PL) depolarization dynamics.

Very recently, a great deal of attention has been drawn to BL TMDs from theoretical and experimental aspects [10,20–27]. The theoretical studies show that only the hole with the same spin in the same valley can hop between different layers efficiently in BL TMDs [22,23]. However, it is further claimed that due to the interlayer hopping energy of the hole being smaller than the energy splitting of the valence bands, the interlayer hopping of the hole is markedly suppressed and hence there may exist a spin-layer locking effect in BL TMDs [23]. In this sense, BL TMDs can be treated as two separated ML TMDs, which has been used to understand the recent experiments related to the optical exciton excitation and PL depolarization dynamics [20,21,23–27].

Experimentally, the optical exciton spectra and related PL depolarization dynamics in BL TMDs are in active progress [10,20–27]. The recent PL experiments in BL TMDs show that the spectra of the optical excitation are very different from the ML situation [24–28]. On one hand, in the BL TMD heterostructures, excitation energy much lower than the one in ML TMDs is observed and attributed to be CT exciton, whose lifetime is found to be as long as nanoseconds [25,26]. On

*Author to whom correspondence should be addressed: mwwu@ustc.edu.cn.

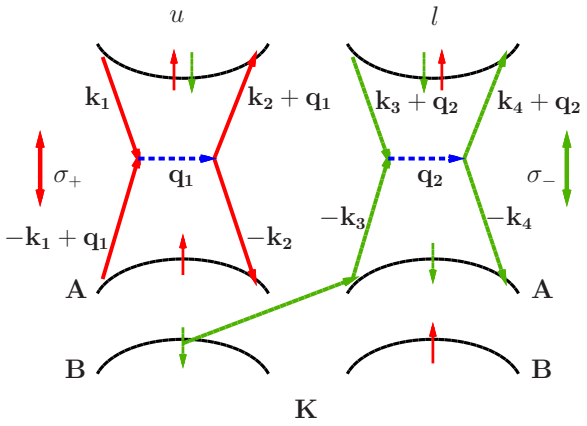

FIG. 1. (Color online) Schematic diagram of the exciton configurations and the intravalley exchange interaction processes for the bright exciton in the K valley for BL TMDs. In the figure, u and l represent "upper" and "lower" layer, respectively, which is associated with the absorption of σ_+ and σ_- light directly in the K valley. A and B denote that the A and B IL (CT) exciton if the e-h pair, which is labeled by the same color, is in the same u/l (different) layer. The Feynman diagrams show the two dominant exciton exchange interaction progresses, with momentum conservation explicitly shown in the figure. On one hand, the e-h pair in one IL exciton can virtually recombine and then generate another IL exciton due to the Coulomb interaction directly, shown by the red arrows. On the other hand, there exists another higher-order process, in which the hole in the CT exciton first hops from one layer to another and then recombines virtually with the electron part to generate the IL exciton due to the Coulomb interaction, shown by the green arrows.

the other hand, in the experiments for the BL WS_2 carried out by Zhu *et al.* [27,28], it has been observed that there are four resonance excitations with excitation energies approximately being 1.68, 1.93, 1.99, and 2.37 eV, respectively, rather than the two excitations named A and B excitons with resonance energies approximately being 2.03 and 2.40 eV in the ML WS_2. These four excitations are speculated to be the indirect exciton for the Γ valley, trion, A exciton, and B exciton excitations, respectively [27,28]. Specifically, compared to the ML WS_2, the obvious redshift for the A exciton energy about 30 ∼ 50 meV is observed in the BL WS_2 in these experiments [27,28]. Moreover, in the work of Zhao *et al.* [24], the additional lowest excitations for the BL MoS_2, WS_2, and WSe_2 are also reported and claimed to be the indirect excitation in the Γ valley, which is in contrast to the understanding in the BL TMD heterostructures [25,26]. Furthermore, the behavior of the PL depolarization dynamics for the BL WS_2 is revealed to be very different from the ML situation [27]. Zhu *et al.* has observed that with the same experimental conditions, the steady-state PL polarization for the excitation 1.99 eV (so-called A exciton) is nearly 100% in the BL WS_2, which is anomalously larger than the one measured in the ML WS_2 (less than 40%) [27]. However, based on the spin-layer locking picture [23], this PL depolarization dynamics is very hard to understand according to the previous study in ML TMDs [31,32], where the intrinsic electron-hole (e-h) exchange interaction can cause efficient PL depolarization due to the Maialle-Silva-Sham (MSS) mechanism [27,33,34].

In this paper, we present a possible understanding of the above observations that is different from the above speculations [24–28]. In our picture, the speculated indirect exciton, which involves a high-order phonon absorption/emission process, is unnecessary. In BL TMDs, due to the strong Coulomb interaction [28,35–39], the e-h pair can form not only the IL exciton but also the CT one. Furthermore, due to the interlayer hopping of the hole, the IL and CT excitons can couple together to form the excimer [29,30]. Here, although the dark exciton can also contribute to the formation of the excimer state, on one hand, it has negligible influence on the excimer energy level; on the other hand, it cannot be excited in the optical process. Hence, in the optical process, only the bright exciton needs to be considered. Furthermore, in the BL WS_2, although there exists large energy splitting for the valence bands, due to the anisotropy of the dielectric constant [8,40–42], the A IL and B CT exciton states are nearly degenerate and hence can couple together to form the A′ and B′ excimer states with the energy level calculated to be 1.99 and 2.10 eV, respectively. Accordingly, the binding energy for the excimer states is calculated to be 40 meV, showing good agreement with the observed redshift for the A exciton in the BL WS_2 [27,28]. Moreover, the energy levels for the lowest and highest excitations are calculated to be 1.69 and 2.41 eV, which correspond to the A CT and B IL excitons, also showing good agreement with the experiment [24,27,28]. Therefore, according to our calculation, the understanding of the four excitations is different from the speculation in the experiments, with the lowest three excitations being the A CT exciton, A′ excimer, and B′ excimer rather than the indirect excitation for the Γ valley, trion, and A exciton [24,27,28].

We further study the exchange interaction between the two excimer states that we reveal in the BL WS_2, based on which we perform the investigation of the PL depolarization dynamics by the kinetic spin Bloch equations (KSBEs) in the pump-probe setup [43,44]. We find that both the Coulomb interaction and interlayer hopping of the hole can contribute to the exchange interaction in both the intra- and intervalley situations. These dominant processes are illustrated in Fig. 1 for the intravalley situation. On one hand, the e-h pair in one IL exciton can virtually recombine and then generate another IL exciton due to the Coulomb interaction directly. On the other hand, there exists another higher-order process, in which the hole in the CT exciton first hops from one layer to another and then recombines virtually with the electron part to generate the IL exciton due to the Coulomb interaction. These exciton transition processes can cause the excimer transition efficiently due to the MSS mechanism [27,31–34], with the former process being more important than the latter.

We then perform the investigation of the PL depolarization dynamics by the KSBEs in the pump-probe setup [43,44]. The calculations based on the KSBEs show that with the absorption of the σ_+ light, the emergence of the σ_- light can be instantaneous, which is similar to ML TMDs [31,45–47]. Furthermore, there is always an anomalous residual PL polarization as large as 50% exactly, lasting for an extremely long time, which is robust against the initial energy broadening and strength of the momentum scattering. This indicates that the PL depolarization time τ_s can be much longer than the excimer lifetime τ_r, which is on the order of picoseconds [19,27,45,48].

Accordingly, based on the rate equation [4,10,11,19], this provides a reasonable explanation for the anomalously large steady-state PL polarization nearly 100% observed in the experiment of Zhu *et al.* in the BL WS_2 [27]. We further reveal that this anomalous *steady state* originates from the specific form of the exchange interaction Hamiltonian. It is interesting to see that there exists a density matrix in the steady state but with residual PL polarization, which can commute with the exchange interaction Hamiltonian and hence protects the large residual PL polarization. Moreover, for the system pumped by the elliptically polarized light, we demonstrate that the residual PL polarization is always half of the initial polarization of the elliptically polarized light.

This paper is organized as follows. In Sec. II, we set up the model and lay out the formalism. In Sec. II A, we derive the excimer state and calculate the excimer excitation energy. In Sec. II B, we derive the excimer exchange interaction. In Sec. III, we present the KSBEs and perform the calculations for the PL depolarization dynamics in the pump-probe setup. We conclude and discuss in Sec. IV.

II. MODEL AND FORMALISM

In this section, following the previous works within the framework of effective-mass approximation [31,33,49,50], the excimer Hamiltonian for the envelope wave function is derived [refer to Eq. (A3) in Appendix A]. Based on the excimer Hamiltonian, we then calculate the energy spectra of the optical excitations (Sec. II A) and the exchange interaction between the excimer states (Sec. II B) in the BL WS_2.

A. Excimer state in BL WS_2

In this subsection, we present the optical excitations in the BL WS_2. Due to the strong Coulomb interaction, the e-h pair forms the IL and CT excitons. Furthermore, due to the efficient interlayer hopping of the hole, the excimer state can be formed from the superposition of the IL and CT exciton states. Here, although the dark exciton can also contribute to the formation of the excimer state, on one hand, it has negligible influence on the excimer energy level; on the other hand, it cannot be excited in the optical process. Hence, in the optical process, only the bright exciton is considered and the corresponding excimer state is referred to as the bright excimer. Specifically, for the optical excitation experiment with one photon process, we focus on the excimer ground state ($1s$-state) $|mn;mn';\mathbf{P}=0\rangle$ ($\mathbf{P}$ is the center-of-mass momentum), which is written as

$$\langle \mathbf{r}_1,\mathbf{r}_2|mn;mn';\mathbf{P}=0\rangle = A_{1s}^{mn} f_{1s}^{mn}(\mathbf{r}_1-\mathbf{r}_2)\Psi_m(\mathbf{r}_1)\tilde{\Psi}_n(\mathbf{r}_2) + A_{1s}^{mn'} f_{1s}^{mn'}(\mathbf{r}_1-\mathbf{r}_2)\Psi_m(\mathbf{r}_1)\tilde{\Psi}_{n'}(\mathbf{r}_2) \quad (1)$$

in the coordinate representation, with the first (second) term on the right-hand side of Eq. (1) describing the IL (CT) exciton wave function. Here, $\mathbf{r}_1$ and $\mathbf{r}_2$ are the electron and hole coordinates. m in the conduction band and n (n') in the valence band denotes the indices including the layer, valley, and spin degrees of the electron; n and n' are limited in the same valley and different layers with the spin degrees being the same as the one in m. A_{1s}^{mn} and $A_{1s}^{mn'}$ represent the amplitudes of the IL and CT exciton states in the excimer state. Within the framework of the effective-mass approximation, $f_{1s}^{mn(n')}(\mathbf{r}_1-\mathbf{r}_2)$ is derived to be the two-dimensional hydrogen-like exciton state (Appendix A) [33], which has also been used in the ML TMDs [8,31,32]. Specifically, for the electron and hole sitting in the m and $n(n')$ band, when the center-of-mass momentum $\mathbf{P}$=0, it is written as

$$f_{1s}^{mn(n')}(\mathbf{r}_1-\mathbf{r}_2)=\sqrt{8/\pi a_{B\square}^2}\exp(-2|\mathbf{r}_1-\mathbf{r}_2|/a_{B\square}), \quad (2)$$

with $a_{B\square}$ being the Bohr radii for the exciton, which are different for the IL and CT excitons represented by $a_{B\parallel}$ and $a_{B\perp}$, respectively, due to the anisotropy of the dielectric constant [8,40–42]. In the following, the hydrogen-like exciton state for the IL and CT excitons are further explicitly represented by $f_{1s}^{\mathrm{IL}}(\mathbf{r}_1-\mathbf{r}_2)$ and $f_{1s}^{\mathrm{CT}}(\mathbf{r}_1-\mathbf{r}_2)$. $\Psi_m(\mathbf{r})$ [$\tilde{\Psi}_{n(n')}(\mathbf{r})$] is the band-edge wave function for the electron (hole) [31,33,49,50].

From Eq. (A3), the amplitudes $A_{1s}^{mn(n')}$ satisfy the equation

$$\left(E_m-E_n+E_{1s}^{mn}\right)A_{1s}^{mn}+\sum_{n'}\tilde{T}_{nn'}A_{1s}^{mn'}=EA_{1s}^{mn}, \quad (3)$$

with E_m and E_n being the band-edge energies for the m and n band, respectively; E_{1s}^{mn} represents the exciton binding energy for the m-band electron and n-band hole, which is further denoted by $E_{b,\parallel}$ and $E_{b,\perp}$ for the IL and CT excitons; $\tilde{T}_{nn'}$ stands for the effective hopping energy for the hole between n and n' band, which only exists for the hole in the same valley with the same spin between different layers. This effective hopping energy $\tilde{T}_{nn'}$ for the hole is determined by the overlap of the IL and CT hydrogen-like exciton wave functions, written as

$$\tilde{T}_{nn'}\equiv t_\perp^*=t_\perp\int d\mathbf{r}_1 d\mathbf{r}_2 f_{1s}^{mn}(\mathbf{r}_1-\mathbf{r}_2)f_{1s}^{mn'}(\mathbf{r}_1-\mathbf{r}_2) = 4t_\perp a_{B\parallel}a_{B\perp}/(a_{B\parallel}+a_{B\perp})^2, \quad (4)$$

with $t_\perp$ being the interlayer hoping energy for the hole [22,23]. Finally, the eigenequations [Eq. (3)] for the amplitudes of the IL (A_{1s}^{mn}) and CT ($A_{1s}^{mn'}$) excitons in the excimer state are written in the matrix form as

$$\begin{pmatrix} E_1-E & \tilde{T}_{nn'} \\ \tilde{T}_{n'n} & E_2-E \end{pmatrix}\begin{pmatrix} A_{1s}^{mn} \\ A_{1s}^{mn'} \end{pmatrix}=0. \quad (5)$$

Here, $E_1=E_m-E_n+E_{b,\parallel}$ and $E_2=E_m-E_{n'}+E_{b,\perp}$ stand for the energy levels for the IL and CT excitons, respectively. Specifically, there are 16 configurations for the bright exciton states in BL TMDs, in which the 4 degenerate A or B IL (CT) excitons are distinguished by the valley and layer degrees of freedom. Therefore, actually there are only four kinds of bright exciton states and hence two kinds of bright excimer states needed to be considered. One excimer state is composed of the A IL and B CT excitons and the other one is composed of the B IL and A CT excitons. Obviously, although there exists large energy splitting for the valence bands, by considering different binding energies E_{1s}^{mn} and $E_{1s}^{mn'}$ for the IL and CT excitons due to the anisotropy of the dielectric constant [8,40–42], the energy levels E_1 and E_2 for the IL and CT excitons can be close to each other.

TABLE I. Material parameters for the calculation of the excimer state and excitation energy.

	MoS_2	WS_2	$MoSe_2$	WSe_2
$\kappa_\parallel$	4.8	4.4	6.9	4.5
$\kappa_\perp$	3.0	2.9	3.8	2.9
κ	3.8	3.6	5.1	3.6
$E_{b,\parallel}$ (meV)	570[a]	700[b]	550[c]	600[d]
$E_{b,\perp}$ (meV)	909	1046	1007	938
$a_{B\parallel}$ (Å)	10.5	9.4	13.9	10.7
$a_{B\perp}$ (Å)	8.3	7.7	5.6	8.5
$2t_\perp$ (meV)	86	109	106	134
$2t_\perp^*$ (meV)	79	102	101	124
E_g (eV)	2.5[a]	2.73[b]	2.18[c]	2.4[d]
$2\lambda_v$ (meV)	147	380[b]	182	420[d]

[a]Reference [35].
[b]References [28,36,37].
[c]Reference [38].
[d]Reference [39].

From Eq. (5), by assuming $E_1 < E_2$, the eigenvalues, which denote the excimer excitation energies, are written as

$$\begin{cases} E_{1'} = \dfrac{E_1+E_2}{2} - \dfrac{1}{2}\sqrt{(E_1-E_2)^2+4|t_\perp^*|^2}, \\ E_{2'} = \dfrac{E_1+E_2}{2} + \dfrac{1}{2}\sqrt{(E_1-E_2)^2+4|t_\perp^*|^2}. \end{cases} \tag{6}$$

Hence the IL and CT excitons can couple together and the excimer state is formed when $|E_1 - E_2| \ll 2t_\perp^*$. Accordingly, the amplitudes $A_{i'}^{\mathrm{IL(CT)}}$ of the IL (CT) exciton state in the excimer state with excitation energy $E_{i'}$ are expressed as

$$\begin{cases} A_{i'}^{\mathrm{IL}} = \dfrac{t_\perp^*}{\sqrt{(t_\perp^*)^2+(E_i-E_{i'})^2}}, \\ A_{i'}^{\mathrm{CT}} = \dfrac{E_{i'}-E_i}{\sqrt{(t_\perp^*)^2+(E_i-E_{i'})^2}}. \end{cases} \tag{7}$$

In the following, we first list the material parameters used in the calculation of excimer state, shown in Table I [22,23,28,35–39,41]. In Table I, the dielectric constants for the IL and CT exciton are denoted by $\kappa_\parallel$ and $\kappa = \sqrt{\kappa_\parallel \kappa_\perp}$, respectively [8,40–42], where $\kappa_\parallel$ and $\kappa_\perp$ represent the dielectric constants parallel and perpendicular to the layer, respectively. Accordingly, by using the binding energy of the IL exciton $E_{b,\parallel}$ directly measured from the experiments in ML TMDs [28,35–39], the binding energy of the CT exciton $E_{b,\perp}$ and the exciton Bohr radius $a_{B\parallel}$ ($a_{B\perp}$) for the IL (CT) exciton are calculated, as shown in Table I [8]. Furthermore, the effective hopping energy for the hole $t_\perp^*$ is determined according to Eq. (4) with $t_\perp$ known [22,23]. The experimentally measured energy gap between the lowest conduction band and highest valence band [28,35–39] and energy splitting for the valence bands are also listed in Table I [22,23,28,36,37,39].

Based on the material parameters in Table I, for the BL WS_2, the energy levels E_1 and E_2 for the IL and CT excitons are further calculated, shown in Table II. In Table II, the two kinds of excimer states in BL TMDs are further represented by $|\mathrm{IL}_A;\mathrm{CT}_B\rangle$ and $|\mathrm{IL}_B;\mathrm{CT}_A\rangle$, respectively. We then calculate the optical excitation energies $E_{1'}$ and $E_{2'}$ for the excimer from Eq. (6), and the corresponding amplitudes $A_{1'}^{\mathrm{IL(CT)}}$ and $A_{2'}^{\mathrm{IL(CT)}}$ of the IL (CT) exciton in the excimer state from Eq. (7), as shown in Table II.

TABLE II. Energy levels and the amplitudes for the IL and CT excitons for the excimer state in the BL WS_2. E_1 and E_2 are the energy levels for the corresponding IL and CT excitons in the excimer states; $E_{1'}$ and $E_{2'}$ are the optical excitation energies for the excimer with $A_{1'}^{\mathrm{IL(CT)}}$ and $A_{2'}^{\mathrm{IL(CT)}}$ being the corresponding amplitudes of the IL (CT) exciton.

	$\lvert\mathrm{IL}_A;\mathrm{CT}_B\rangle$	$\lvert\mathrm{IL}_B;\mathrm{CT}_A\rangle$
E_1 (eV)	2.41	2.03
E_2 (eV)	1.69	2.06
$E_{1'}$ (eV)	2.41	1.99
$E_{2'}$ (eV)	1.69	2.10
$A_{1'}^{\mathrm{IL}}$	1.0	0.79
$A_{1'}^{\mathrm{CT}}$	0.0	-0.62
$A_{2'}^{\mathrm{IL}}$	0.0	0.62
$A_{2'}^{\mathrm{CT}}$	1.0	0.79

From the results in Table II, it can be seen that there are four optical excitations in the BL WS_2, whose energy levels are calculated to be 1.69, 1.99, 2.10, and 2.41 eV, respectively. On one hand, for the lowest (highest) energy level 1.69 (2.41) eV, it can be seen from the amplitude $A_{2'}^{\mathrm{CT}} \approx 1$ ($A_{1'}^{\mathrm{IL}} \approx 1$) that the excitation state is actually the A CT (B IL) exciton state. On the other hand, the energy levels $E_1 = 2.03$ eV for the A IL exciton and $E_2 = 2.06$ eV for the B CT exciton are very close ($|E_1 - E_2| \ll 2t_\perp^*$), and hence the A′ and B′ excimer states corresponding to $E_1' = 1.99$ and $E_2' = 2.10$ eV form due to the efficient interlayer hopping of the hole. Accordingly, the binding energy for the A′ excimer state is calculated to be $|E_1 - E_1'| = 40$ meV. Our calculated results show good agreement with the recent experiments in BL WS_2 [24,27,28].

In the experiment of Zhu *et al.* for the BL WS_2 [27], it has been observed that there are four resonant excitations with excitation energies approximately being 1.68, 1.93, 1.99, and 2.37 eV, in good agreement with our calculation with 1.69, 1.99, 2.10, and 2.41 eV [24]. However, in the experiments [24,27,28], these four excitations have been speculated to be the indirect exciton for the Γ valley, trion, A exciton, and B exciton excitations, respectively. According to our theory, these four excitations are the A CT exciton, A′ excimer, B′ excimer, and B IL exciton, in consistence with the understanding in the BL TMD heterostructures [25,26]. Furthermore, compared to the ML WS_2, the obvious redshift for the A exciton about 30 ∼ 50 meV is observed in the BL WS_2 in these experiments [27,28], which also confirms our calculated binding energy 40 meV for the A′ excimer.

Finally, we address that the interlayer hopping energy for the hole can be tuned by variation of the interlayer distance [29], which can be realized in high-pressure experiments [30,51]. Hence, the energy levels of the A′ and B′ excimer states can be tuned by means of the pressure in BL WS_2 and other BL TMDs, which can be observed in the experiment directly [30,51].

B. Exchange interaction between excimer states

We further show the exchange interaction between the excimer states in BL TMDs (refer to Appendix A)

[31,33,49,49,50]. With the IL and CT exciton states with center-of-mass $\mathbf{P}$ expressed as $|mn;\mathbf{P}\rangle$ and $|mn';\mathbf{P}\rangle$ in Eq. (1), for simplicity, the excimer state is further represented as

$$|mn;mn';\mathbf{P}\rangle = A_{1s}^{mn}|mn;\mathbf{P}\rangle + A_{1s}^{mn'}|mn';\mathbf{P}\rangle. \tag{8}$$

Accordingly, the exchange interaction between the two excimer states $|m_1n_1;m_1n_1';\mathbf{P}\rangle$ and $|m_2n_2;m_2n_2';\mathbf{P}'\rangle$ can be obtained from the exchange interaction between the exciton states, which only exists between the *bright* ones [31,32],

$$\begin{aligned}
&\langle m_2n_2;m_2n_2';\mathbf{P}'|H^{\rm ex}|m_1n_1;m_1n_1';\mathbf{P}\rangle \\
&= \left(A_{1s}^{m_2n_2}\right)^* A_{1s}^{m_1n_1}\langle m_2n_2;\mathbf{P}'|H^{\rm ex}|m_1n_1;\mathbf{P}\rangle \\
&\quad + \left(A_{1s}^{m_2n_2}\right)^* A_{1s}^{m_1n_1'}\langle m_2n_2;\mathbf{P}'|H^{\rm ex}|m_1n_1';\mathbf{P}\rangle \\
&\quad + \left(A_{1s}^{m_2n_2'}\right)^* A_{1s}^{m_1n_1}\langle m_2n_2';\mathbf{P}'|H^{\rm ex}|m_1n_1;\mathbf{P}\rangle \\
&\quad + \left(A_{1s}^{m_2n_2'}\right)^* A_{1s}^{m_1n_1'}\langle m_2n_2';\mathbf{P}'|H^{\rm ex}|m_1n_1';\mathbf{P}\rangle.
\end{aligned} \tag{9}$$

On the right-hand side of Eq. (9), the first (last) term describes the exchange interaction between the two IL (CT) exciton states, whereas the second and third terms show the exchange interaction between the IL and CT exciton states. These exchange interactions between the bright exciton states include both the long-rang (L-R) and short-range (S-R) parts, with the latter one usually being one order of magnitude smaller than the former in semiconductors [52]. For the L-R part in Eq. (9), as shown later, the first term is one order of magnitude larger than the second and third terms, whereas the second and third terms are one order of magnitude larger than the last one. For the S-R part, the exchange interaction between the IL exciton states (the first term) is on the same order as the L-R one between the IL and CT excitons (the second and third terms). Here, we only show the explicit form for the exchange interaction in the same order as the L-R one between the IL and CT excitons, which are dominant in the exchange interaction between the excimers (the second and third terms).

With the initial and final exciton states being the IL bright exciton states, the exchange interaction describes the virtual recombination of the e-h pair in one IL bright exciton state and then generation of another IL bright one due to the Coulomb interaction directly (as shown in Fig. 1). The L-R (S-R) exchange interaction is written as [given in Eq. (A11) in Appendix A]

$$H^{L(1)}_{\substack{m'n'\\mn}} = \frac{e^2}{2\varepsilon_0\kappa_\parallel|\mathbf{P}|}\delta_{\mathbf{P},\mathbf{P}'}\left[f^{\rm IL}_{1s}(0)\right]^* f^{\rm IL}_{1s}(0)Q^{(1)}_{\substack{m'n'\\mn}}(\mathbf{P}), \tag{10}$$

where

$$\begin{aligned}
Q^{(1)}_{\substack{m'n'\\mn}}(\mathbf{P}) = \frac{\hbar^2}{2m_0^2}&\left[\frac{1}{(E_m-E_n)^2}+\frac{1}{(E_{m'}-E_{n'})^2}\right] \\
&\times(\mathbf{P}\cdot\boldsymbol{\pi}_{m'\Theta n'})(\mathbf{P}\cdot\boldsymbol{\pi}_{\Theta nm}).
\end{aligned} \tag{11}$$

Here, m_0 is the free electron mass, ε_0 stands for the vacuum permittivity, and $\boldsymbol{\pi}_{m'\Theta n'}$ and $\boldsymbol{\pi}_{\Theta nm}$ come from the $\mathbf{k}\cdot\mathbf{p}$ matrix elements in the Hamiltonian [Eq. (A1)] with Θ being the time reversal operator (refer to Appendix A).

With the IL bright exciton states shown in the order $|\uparrow^u_{\rm Kc},\uparrow^u_{\rm Kv}\rangle$, $|\downarrow^u_{\rm Kc},\downarrow^u_{\rm Kv}\rangle$, $|\uparrow^l_{\rm Kc},\uparrow^l_{\rm Kv}\rangle$, $|\downarrow^l_{\rm Kc},\downarrow^l_{\rm Kv}\rangle$, $|\uparrow^u_{\rm K'c},\uparrow^u_{\rm K'v}\rangle$, $|\downarrow^u_{\rm K'c},\downarrow^u_{\rm K'v}\rangle$, $|\uparrow^l_{\rm K'c},\uparrow^l_{\rm K'v}\rangle$, and $|\downarrow^l_{\rm K'c},\downarrow^l_{\rm K'v}\rangle$, according to Eq. (10), the exchange interaction matrix between the above IL bright exciton states $|m_1n_1;\mathbf{P}\rangle$ and $|m_2n_2;\mathbf{P}'\rangle$ reads

$$H^{(1)}_{\rm ex} = \frac{C\delta_{\mathbf{P},\mathbf{P}'}}{|\mathbf{P}|}\begin{pmatrix}
\alpha_1|\mathbf{P}|^2 & \beta|\mathbf{P}|^2 & \beta P_+^2 & \alpha_1 P_+^2 & -\beta P_+^2 & -\alpha_1 P_+^2 & -\alpha_1|\mathbf{P}|^2 & -\beta|\mathbf{P}|^2 \\
 & \alpha_2|\mathbf{P}|^2 & \alpha_2 P_+^2 & \beta P_+^2 & -\alpha_2 P_+^2 & -\beta P_+^2 & -\beta|\mathbf{P}|^2 & -\alpha_2|\mathbf{P}|^2 \\
 & & \alpha_2|\mathbf{P}|^2 & \beta|\mathbf{P}|^2 & -\alpha_2|\mathbf{P}|^2 & -\beta|\mathbf{P}|^2 & -\beta P_-^2 & -\alpha_2 P_-^2 \\
 & & & \alpha_1|\mathbf{P}|^2 & -\beta|\mathbf{P}|^2 & -\alpha_1|\mathbf{P}|^2 & -\alpha_1 P_-^2 & -\beta P_-^2 \\
 & & & & \alpha_2|\mathbf{P}|^2 & \beta|\mathbf{P}|^2 & \beta P_-^2 & \alpha_2 P_-^2 \\
 & & & & & \alpha_1|\mathbf{P}|^2 & \alpha_1 P_-^2 & \beta P_-^2 \\
 & & & & & & \alpha_1|\mathbf{P}|^2 & \beta|\mathbf{P}|^2 \\
 & & & & & & & \alpha_2|\mathbf{P}|^2
\end{pmatrix}. \tag{12}$$

Here, $C = e^2/(2\varepsilon_0\kappa_\parallel)|f^{\rm IL}_{1s}(0)|^2$; $P_\pm = P_x \pm iP_y$; and the material parameters $\alpha_1 = a^2t^2/(\Delta-\lambda_c+\lambda_v)^2$, $\alpha_2 = a^2t^2/(\Delta+\lambda_c-\lambda_v)^2$, and $\beta = \frac{1}{2}[\frac{a^2t^2}{(\Delta+\lambda_c-\lambda_v)^2}+\frac{a^2t^2}{(\Delta-\lambda_c+\lambda_v)^2}]$ are calculated according to the parameters in Ref. [22] with λ_c representing the splitting of the conduction band, shown in Table III for the BL MoS_2, WS_2, $MoSe_2$, and WSe_2.

With the initial and final exciton states being the CT and IL exciton states, the exchange interaction describes the process that the hole in the CT exciton first hops from one layer to another and then recombines virtually with the electron part to generate the IL exciton due to the Coulomb interaction. Hence, this process [Eq. (13)] for the L-R exchange interaction is on the order of $t_\perp^*/E_g$ times of the former L-R one [Eq. (10)]. This L-R exchange interaction is expressed as

$$H^{L(2)}_{\substack{m'n'\\mn}} = \frac{e^2}{2\varepsilon_0\kappa_\parallel|\mathbf{P}|}\delta_{\mathbf{P},\mathbf{P}'}\left[f^{\rm IL}_{1s}(0)\right]^* f^{\rm CT}_{1s}(0)Q^{(2)}_{\substack{m'n'\\mn}}(\mathbf{P}),$$

TABLE III. Material parameters α_1, α_2, β, $\tilde{\alpha}(\pm1)$, and $\tilde{\beta}(\pm1)$ for the BL MoS_2, WS_2, $MoSe_2$, and WSe_2 with the unit being Å^2.

	α_1	α_2	β	$\tilde{\alpha}(\pm1)$	$\tilde{\beta}(\pm1)$
MoS_2	4.51	3.82	4.16	0.09	0.09
WS_2	6.54	4.43	5.48	0.14	0.14
$MoSe_2$	4.65	3.67	4.16	0.14	0.14
WSe_2	7.39	4.49	5.94	0.21	0.21

where

$$Q^{(2)}_{\substack{m'n'\\ mn}}(\mathbf{P}) = \frac{\hbar^2}{2m_0^2}\frac{(\mathbf{P}\cdot\boldsymbol{\pi}_{m'\Theta n'})(\mathbf{P}\cdot\boldsymbol{\pi}_{\Theta l''m})\tilde{T}_{\Theta n\Theta l''}}{(E_m - E_{l''})(E_m - E_n)}\left(\frac{1}{E_m - E_{l''}} + \frac{1}{E_m - E_n}\right). \tag{13}$$

With the CT exciton states being represented by $|\uparrow^u_{\mathrm{Kc}}, \uparrow^l_{\mathrm{Kv}}\rangle$, $|\downarrow^u_{\mathrm{Kc}}, \downarrow^l_{\mathrm{Kv}}\rangle$, $|\uparrow^l_{\mathrm{Kc}}, \uparrow^u_{\mathrm{Kv}}\rangle$, $|\downarrow^l_{\mathrm{Kc}}, \downarrow^u_{\mathrm{Kv}}\rangle$, $|\uparrow^u_{\mathrm{K'c}}, \uparrow^l_{\mathrm{K'v}}\rangle$, $|\downarrow^u_{\mathrm{K'c}}, \downarrow^l_{\mathrm{K'v}}\rangle$, $|\uparrow^l_{\mathrm{K'c}}, \uparrow^u_{\mathrm{K'v}}\rangle$, and $|\downarrow^l_{\mathrm{K'c}}\downarrow^u_{\mathrm{K'v}}\rangle$, according to Eq. (13), the exchange interaction matrix between the above CT bright exciton and IL bright exciton states $|mn;\mathbf{P}\rangle$ and $|mn';\mathbf{P}'\rangle$ reads

$$H^{(2)}_{\mathrm{ex}} = \frac{C'\delta_{\mathbf{P},\mathbf{P}'}}{|\mathbf{P}|}\begin{pmatrix}
\tilde{\alpha}(1)|\mathbf{P}|^2 & \tilde{\beta}(1)|\mathbf{P}|^2 & \tilde{\beta}(-1)P_+^2 & \tilde{\alpha}(-1)P_+^2 & -\tilde{\beta}(1)P_+^2 & -\tilde{\alpha}(1)P_+^2 & -\tilde{\alpha}(-1)|\mathbf{P}|^2 & -\tilde{\beta}(-1)|\mathbf{P}|^2 \\
 & \tilde{\beta}(1)|\mathbf{P}|^2 & \tilde{\beta}(-1)P_+^2 & \tilde{\alpha}(-1)P_+^2 & -\tilde{\beta}(1)P_+^2 & -\tilde{\alpha}(1)P_+^2 & -\tilde{\alpha}(-1)|\mathbf{P}|^2 & -\tilde{\beta}(-1)|\mathbf{P}|^2 \\
 & & \tilde{\beta}(-1)|\mathbf{P}|^2 & \tilde{\alpha}(-1)|\mathbf{P}|^2 & -\tilde{\beta}(1)|\mathbf{P}|^2 & -\tilde{\alpha}(1)|\mathbf{P}|^2 & -\tilde{\alpha}(-1)P_-^2 & -\tilde{\beta}(-1)P_-^2 \\
 & & & \tilde{\alpha}(-1)|\mathbf{P}|^2 & -\tilde{\beta}(1)|\mathbf{P}|^2 & -\tilde{\alpha}(1)|\mathbf{P}|^2 & -\tilde{\alpha}(-1)P_-^2 & -\tilde{\beta}(-1)P_-^2 \\
 & & & & \tilde{\beta}(1)|\mathbf{P}|^2 & \tilde{\alpha}(1)|\mathbf{P}|^2 & \tilde{\alpha}(-1)P_-^2 & \tilde{\beta}(-1)P_-^2 \\
 & & & & & \tilde{\alpha}(1)|\mathbf{P}|^2 & \tilde{\alpha}(-1)P_-^2 & \tilde{\beta}(-1)P_-^2 \\
 & & & & & & \tilde{\alpha}(-1)|\mathbf{P}|^2 & \tilde{\beta}(-1)|\mathbf{P}|^2 \\
 & & & & & & & \tilde{\beta}(-1)|\mathbf{P}|^2
\end{pmatrix}. \tag{14}$$

Here, $C' = e^2/(2\varepsilon_0\kappa_\parallel)[f^{\mathrm{IL}}_{1s}(0)]^* f^{\mathrm{CT}}_{1s}(0)$. The parameters

$$\tilde{\alpha}(\tau) = \frac{a^2t^2\tau_\perp^*(\Delta - \lambda_c + \tau Ed/2)}{(\Delta - \lambda_c + \lambda_v)^2(\Delta - \lambda_c - \lambda_v + \tau Ed)^2} \tag{15}$$

and

$$\tilde{\beta}(\tau) = \frac{a^2t^2\tau_\perp^*(\Delta + \lambda_c + \tau Ed/2)}{(\Delta + \lambda_c - \lambda_v)^2(\Delta + \lambda_c + \lambda_v + \tau Ed)^2}, \tag{16}$$

with E and d being the magnitude of the electric field and the interlayer distance, respectively. Specifically, one observes that the form of Eq. (14) is very similar to the one of Eq. (12), with the magnitude of the former [Eq. (14)] being one order smaller than the latter [Eq. (12)]. $\tilde{\alpha}(\tau)$ and $\tilde{\beta}(\tau)$ are calculated with the material parameters taken from Ref. [22] for $E = 0$, shown in Table III for the BL MoS_2, WS_2, $MoSe_2$, and WSe_2.

From Eqs. (12) and (14), both the intra- and intervalley exchange interactions can cause the bright excimer transition due to the MSS mechanism [33,34]. However, if the energy levels for the two excimer states have large splitting, the excimer transition is nearly forbidden due to the detuning effect [53]. Hence, in the BL WS_2, by considering the large energy splitting about 100 meV for the A′ and B′ excimer states, we only need to consider the transition between the degenerate excimer states [27].

III. PL DEPOLARIZATION DUE TO e-h EXCHANGE INTERACTION

In this section, we focus on the PL depolarization due to the e-h exchange interaction based on the KSBEs in the BL WS_2. We first present the model and then study the PL depolarization dynamics in the pump-probe setup.

A. Model and KSBEs

We focus on the four degenerate A′ bright excimer states ($E_1' = 1.99$ eV) according to the experiment condition in the work of Zhu *et al.* [27], which are represented as $|\downarrow^u_{\mathrm{Kc}}, \downarrow^u_{\mathrm{Kv}}; \downarrow^u_{\mathrm{Kc}}, \downarrow^l_{\mathrm{Kv}}; \mathbf{P}\rangle$, $|\uparrow^l_{\mathrm{Kc}}, \uparrow^l_{\mathrm{Kv}}; \uparrow^l_{\mathrm{Kc}}, \uparrow^u_{\mathrm{Kv}}; \mathbf{P}\rangle$, $|\uparrow^u_{\mathrm{K'c}}, \uparrow^u_{\mathrm{K'v}}; \uparrow^u_{\mathrm{K'c}}, \uparrow^l_{\mathrm{K'v}}; \mathbf{P}\rangle$, and $|\downarrow^l_{\mathrm{K'c}}, \downarrow^l_{\mathrm{K'v}}; \downarrow^l_{\mathrm{K'c}}, \downarrow^u_{\mathrm{K'v}}; \mathbf{P}\rangle$. According to chiral optical valley selection rule [22], the first and fourth (second and third) states are associated with σ_+ (σ_-) light. From Eqs. (12) and (14), the L-R exchange interaction between the four excimer states is written as

$$H_{\mathrm{ex}}(\mathbf{P}) \approx \frac{C''\delta_{\mathbf{P},\mathbf{P}'}}{|\mathbf{P}|}\begin{pmatrix}
|\mathbf{P}|^2 & P_+^2 & -P_+^2 & -|\mathbf{P}|^2 \\
P_-^2 & |\mathbf{P}|^2 & -|\mathbf{P}|^2 & -P_-^2 \\
-P_-^2 & -|\mathbf{P}|^2 & |\mathbf{P}|^2 & P_-^2 \\
-|\mathbf{P}|^2 & -P_+^2 & P_+^2 & |\mathbf{P}|^2
\end{pmatrix}. \tag{17}$$

Here, $C'' = |A^{\mathrm{IL}}_{1'}|^2 C\alpha_2 + 2A^{\mathrm{IL}}_{1'}A^{\mathrm{CT}}_{1'}C'\tilde{\beta}(\pm 1)$.

With the exchange interaction Hamiltonian [Eq. (17)], the PL depolarization dynamics associated with the A′ bright excimers ($E_1' = 1.99$ eV) can be described by the KSBEs [33,34,43,44]:

$$\partial_t\rho(\mathbf{P},t) = \partial_t\rho(\mathbf{P},t)|_{\mathrm{coh}} + \partial_t\rho(\mathbf{P},t)|_{\mathrm{scat}}. \tag{18}$$

In these equations, $\rho(\mathbf{P},t)$ represent the 4×4 density matrices of the A′ bright excimers with center-of-mass momentum $\mathbf{P}$ at time t, in which the diagonal elements $\rho_{ss}(\mathbf{P},t)$ describe the excimer distribution functions and the off-diagonal elements $\rho_{ss'}(\mathbf{P},t)$ with $s \neq s'$ represent the coherence between different excimer states. In the collinear space, the coherent term is given by

$$\partial_t\rho(\mathbf{P},t)|_{\mathrm{coh}} = -\frac{i}{\hbar}[H_{\mathrm{ex}}, \rho(\mathbf{P},t)], \tag{19}$$

where [,] denotes the commutator. The scattering term $\partial_t\rho(\mathbf{P},t)|_{\mathrm{scat}}$ is written in the elastic approximation as [33]

$$\partial_t\rho(\mathbf{P},t)|_{\mathrm{scat}} = \sum_{\mathbf{P}'} W_{\mathbf{P}\mathbf{P}'}[\rho(\mathbf{P}',t) - \rho(\mathbf{P},t)]. \tag{20}$$

Here, $W_{\mathbf{P}\mathbf{P}'}$ represents the momentum scattering rate.

TABLE IV. Material parameters used in the computation for the KSBEs.

$\kappa_\parallel$	4.4[a]	m^*/m_0	0.21[b]
$a_{B\parallel}$ (nm)	0.94	$a_{B\perp}$ (nm)	0.77
$n_{\rm ex}$ (cm^{-2})	10^{12}	τ_P^* (fs)	13.0[c]
α_2 (Å^2)	4.43	$\beta(\pm1)$ (Å^2)	0.14
$A^{\rm IL}_{1'}$	0.79	$A^{\rm CT}_{2'}$	−0.62

[a]Reference [35].
[b]Reference [54].
[c]Reference [27].

By solving the KSBEs, one obtains the evolution of the PL polarization

$$P(t) = [I(\sigma_+) - I(\sigma_-)]/[I(\sigma_+) + I(\sigma_-)] = \frac{1}{n_{\rm ex}} \sum_{\mathbf{P}} {\rm Tr}[\rho(\mathbf{P},t) I'], \quad (21)$$

with $I(\sigma_\pm)$ representing the intensity of the $\sigma_\pm$ light and $n_{\rm ex}$=$\sum_{\mathbf{P}}{\rm Tr}[\rho(\mathbf{P},t)]$ being the density of the pumped bright excimer:

$$I' = \begin{pmatrix} 1 & 0 & 0 & 0 \\ 0 & -1 & 0 & 0 \\ 0 & 0 & -1 & 0 \\ 0 & 0 & 0 & 1 \end{pmatrix}. \quad (22)$$

The initial condition for the density matrix is set to be

$$\rho_{ss}(\mathbf{P},0) = \alpha_{ss} \exp\{-[\varepsilon(\mathbf{P}) - \varepsilon_{\rm pump}]^2/(2\Gamma^2)\} \quad (23)$$

and $\rho_{ss'}(\mathbf{P},0) = 0$ with $s \neq s'$. Here, $\varepsilon(\mathbf{P}) = \hbar^2|\mathbf{P}|^2/(2m^*)$ is the excimer kinetic energy with m^* being the excimer effective mass, which is the same as the effective mass of the IL and CT excitons; $\varepsilon_{\rm pump}$ is the energy of pulse center in reference to the minimum of the excimer energy band; Γ denotes the energy broadening of the pulse;

$$\alpha_{ss} = \frac{n_{ss}}{\sum_{\mathbf{P}} \exp\{-[\varepsilon(\mathbf{P}) - \varepsilon_{\rm pump}]^2/(2\Gamma^2)\}}, \quad (24)$$

with $n_{\rm ss}$ being the pumped excimer density. In the pump-probe experiment, according to the chiral optical valley selection rule [22], we set $n_{11} = n_{44} = n_{\rm ex}/2$ and $n_{22} = n_{33} = 0$ with $P(0) = 100\%$.

B. PL depolarization dynamics in the pump-probe setup

Then we look into the PL depolarization dynamics in the pump-probe setup in the BL WS_2 [28]. The material parameters in our computation are listed in Table IV.

In our computation, as a first step in the investigation, the momentum relaxation time τ_P^* in Table IV is obtained based on the elastic scattering approximation in the KSBEs [33]. Its value is estimated to be 13 fs by considering the measured broadening of the A exciton energy $\Gamma \approx 55$ meV at 10 K with $\tau_P^* \approx \hbar/\Gamma$ [27,28]. By setting $\varepsilon_{\rm pump} = 0$ eV in Eq. (23) [45–47] with the material parameters in Table IV, the evolution of the PL polarization with different energy broadenings and scattering strengths can be obtained by numerically solving the KSBEs, shown in Fig. 2.

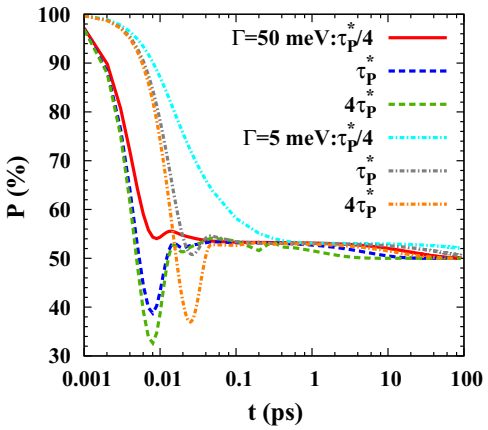

FIG. 2. (Color online) Evolution of the PL polarization when the pumped energy is centered at the resonance energy for the A′ bright excimer ($E_1' = 1.99$ eV) with different energy broadenings ($\Gamma = 50$ and 5 meV) and momentum relaxation times ($\tau_P^*/4$, τ_P^*, and $4\tau_P^*$).

From Fig. 2, several features of the PL depolarization dynamics can be obtained. Similar to the experimental results in ML TMDs [46,47] with the absorption of the σ_+ light, the emergence of the σ_- light is also instantaneous (in the order of 10 fs) when the energy broadening is large ($\Gamma = 50$ meV) or/and the scattering is weak. Moreover, there is also a large residual PL polarization 50%, lasting for an infinitely long time, which is robust against the initial energy broadening and strength of the momentum scattering. This seems similar to the situation in ML TMDs [31,45–47]. However, in the BL WS_2, the mechanism for the existence of this large residual PL polarization is different from the ML situation [31,45–47]. In ML TMDs, the residual PL polarization arises from the weak exchange interaction between the exciton states with $|\mathbf{P}| \approx 0$, in which the decay of the residual PL polarization (about 10%) is nevertheless obvious and lasts only for about 10 ps [31,45–47]. Moreover, the residual PL polarization there is sensitive to the experimental conditions and strength of the scattering. In the following, we show that the anomalous PL depolarization behavior here, which is very different from the spin relaxation in semiconductors [44,55–62], arises from the unique feature of the exchange interaction [Eq. (17)] in the BL WS_2.

It is interesting to see that when the system evolves into the steady state shown in Fig. 2 with $P = 50\%$, the density matrix evolved into has the form

$$\rho_s(\mathbf{P}) = a(\mathbf{P}) \begin{pmatrix} 3/8 & 0 & 0 & 1/8 \\ 0 & 1/8 & -1/8 & 0 \\ 0 & -1/8 & 1/8 & 0 \\ 1/8 & 0 & 0 & 3/8 \end{pmatrix}. \quad (25)$$

Here, $a(\mathbf{P})$ depends on the concrete initial condition [Eq. (23)] and satisfies the normalized condition $\sum_{\mathbf{P}} a(\mathbf{P})/n_{\rm ex} = 1$. One notes that when the system evolves into this steady state [Eq. (25)] with the initial condition $n_{11} = n_{44} = n_{\rm ex}/2$ and $n_{22} = n_{33} = 0$, $(n_{11} + n_{44})/(n_{22} + n_{33}) = 3:1$ is satisfied and $P = \frac{1}{n_{\rm ex}} \sum_{\mathbf{P}} {\rm Tr}[\rho_s(\mathbf{P}) I']$ is calculated to be 50% exactly. Furthermore, when the system is polarized by the σ_- light with the initial condition being $n_{11} = n_{44} = 0$ and

$n_{22} = n_{33} = n_{ex}/2$, we find $(n_{11} + n_{44})/(n_{22} + n_{33}) = 1 : 3$ and $P = -50\%$ in the steady state. Moreover, it is easy to verify that this density matrix commutes with the exchange interaction Hamiltonian [Eq. (17)]

$$[H_{ex}(\mathbf{P}), \rho_s(\mathbf{P})] = 0, \tag{26}$$

with $\rho_s(\mathbf{P})H_{ex}(\mathbf{P}) = H_{ex}(\mathbf{P})\rho_s(\mathbf{P}) = a(\mathbf{P})H_{ex}(\mathbf{P})/4$. Hence, from the KSBEs [Eq. (18)], this guarantees the residual PL polarization is in the steady state.

In Appendix B, we extend our formula to the situation with the system pumped by the elliptically polarized light analytically. With the polarization of the elliptically polarized light being $x = [I(\sigma_+) - I(\sigma_-)]/[I(\sigma_+) + I(\sigma_-)]$, we show that the residual PL polarization is always $x/2$, which is half of the initial polarization of the elliptically polarized light. Furthermore, the steady-state density matrix $\rho_s(\mathbf{P})$ is proved to be

$$\rho_s(\mathbf{P}) = \frac{a(\mathbf{P})}{4}\begin{pmatrix} 1+x/2 & 0 & 0 & x/2 \\ 0 & 1-x/2 & -x/2 & 0 \\ 0 & -x/2 & 1-x/2 & 0 \\ x/2 & 0 & 0 & 1+x/2 \end{pmatrix}. \tag{27}$$

Therefore, the steady-state density matrix Eq. (25) with the system pumped by the σ_+ light ($x = 100\%$) is only a special situation in Eq. (27).

Finally, we address the recent steady-state measurement of the PL polarization by Zhu *et al.* for the BL WS_2, in which the anomalous PL polarization as large as $P \approx 100\%$ is observed [27]. The puzzle of the experiment is that under the same experimental condition, the measured PL polarization in the BL WS_2 is anomalously larger than the ML situation, in which P is less than 40% [27], and hence this cannot be understood by the spin-layer locking picture of Jones *et al.* [22,23]. However, this experiment can be well understood according to our calculation in the BL WS_2 based on the exchange interaction. In the BL WS_2, the PL relaxation time τ_s should be extremely long when the system is at the steady state. Moreover, according to the rate equation [4,10,11,19], the steady-state PL polarization is derived to be

$$P = P_0/(1 + 2\tau_r/\tau_s), \tag{28}$$

with $P_0 \approx 100\%$ being the initial PL polarization. Hence when $\tau_s \gg \tau_r$, we obtain $P \approx 100\%$, whereas in the ML WS_2, it has been well understood that the e-h exchange interaction can cause PL depolarization efficiently [31,32].

IV. CONCLUSION AND DISCUSSION

In conclusion, we have investigated the excimer excitation spectra and the PL depolarization dynamics in BL WS_2. We first present a possible understanding for the optical excitation spectra for the recent PL experiments by Zhu *et al.* in the BL WS_2 [27,28], in which four resonance excitations (1.68, 1.93, 1.99, and 2.37 eV) are observed and speculated to be the indirect exciton for the Γ valley, trion, A exciton, and B exciton excitations, respectively [27,28]. Furthermore, in the experiment [27,28], the redshift for the A exciton energy about $30 \sim 50$ meV is observed when the sample is synthesized from ML to BL. In our study, we find that in the BL WS_2, due to the efficient interlayer hopping of the hole, the excimer states can be formed from the superposition of the IL and CT excitons [8,40–42]. According to our study, the energy levels of the four experimentally observed optical excitations in the BL WS_2 are calculated to be 1.69, 1.99, 2.10, and 2.41 eV, corresponding to A CT exciton, A′ excimer, B′ excimer, and B IL exciton, respectively. Here, the A′ (B′) excimer state is composed of the A IL and B CT exciton states. These calculations show good agreement with the recent experiments by Zhu *et al.* [27,28], but with different understanding for the first three elementary excitations. Furthermore, the binding energy for the A′ excimer state is calculated to be 40 meV, in consistent with $30 \sim 50$ meV observed in the experiment [27,28]. Based on the excimer state, we further derive the e-h exchange interaction including all the dominant processes. With the transition channel between dark excitons forbidden [31,32], we find that both the intra- and intervalley exchange interactions can cause the bright excimer transition due to the MSS mechanism [33,34].

We then study the PL depolarization dynamics due to the e-h exchange interaction in the pump-probe setup based on the KSBEs. We find that with the absorption of the σ_+ light, the emergence of the σ_- light can be instantaneous, which is similar to the ML situation [31,45–47]. Moreover, we further find that there is always a residual PL polarization as large as 50%, lasting for infinitely long time, which is robust against the initial energy broadening and strength of the momentum scattering. This large steady-state PL polarization indicates that the PL relaxation time is extremely long in the BL WS_2 in the steady state and can be the cause of the anomalously large PL polarization nearly 100% observed in the experiment by Zhu *et al.* in the BL WS_2 [27]. This steady state is shown to come from the unique form of the exchange interaction Hamiltonian [Eq. (17)], under which the density matrix evolves into the state $\rho_s(\mathbf{P})$ [Eq. (25)] which communicates with the exchange interaction Hamiltonian $[H_{ex}(\mathbf{P}), \rho_s(\mathbf{P})] = 0$, with $\rho_s(\mathbf{P})H_{ex}(\mathbf{P}) = H_{ex}(\mathbf{P})\rho_s(\mathbf{P}) \propto H_{ex}(\mathbf{P})$. Specifically, from the density matrix $\rho_s(\mathbf{P})$ [Eq. (25)], one further observes that when the system is polarized by the σ_+ light, in the steady state, the density ratio of the bright excimers associated with the σ_+ and σ_- light is 3 : 1; whereas when the system is polarized by the σ_- light, this ratio is 1 : 3. Furthermore, in general, if the system is pumped by the elliptically polarized light, we have demonstrated that the residual PL polarization is always half of the initial polarization of the elliptically polarized light. Moreover, it is noted that although this specific exchange interaction Hamiltonian [Eq. (17)] is derived based on the excimer states, its contribution is mainly from the exchange interaction between the two IL excitons [Eq. (12)].

It should be noted that rather than our approach by dealing first with the strong Coulomb interaction and then the influence of the interlayer hopping of the hole for the excimer state [31,33,49,49,50], Jones *et al.* presented other treatment for the exciton states in BL TMDs by considering the influence of the interlayer hopping of the hole [23]. In their treatment, Jones *et al.* first diagonalize the $\mathbf{k} \cdot \mathbf{p}$ Hamiltonian [Eq. (A1)] and then construct the exciton states with the eigenstates of the Hamiltonian [22,23]. However, due to the fact that the interlayer hopping energy for the hole is smaller than the valence bands energy splitting, the mixture of the

wave function of the holes in different layers is negligible and hence the BL TMDs can be treated as two separated ML TMDs, which is referred to as the spin-layer locking effect in their study [22,23]. However, this treatment is correct only when the strength of the Coulomb interaction is weak, and hence the exciton binding energy is much smaller than the interlayer hopping energy for the hole. Whereas in BL TMDs, the experimentally measured exciton binding energy is much larger than the interlayer hopping energy for the hole [22,23,28,35–39]. Therefore, one should first deal with the Coulomb interaction and then the effect of the interlayer hopping of the hole to get the correct picture for the excitation in BL TMDs, as we do in this study.

Furthermore, there also exists other speculation for the lowest excitation with excitation energy $E \approx 1.68$ eV observed in the BL WS_2 in the literature [24,27]. Zhao *et al.* [24] and Zhu *et al.* [27] claimed that this excitation comes from the indirect excitation for the Γ valley. This claim is still controversial. On one hand, this is in contrast to the understanding in the BL TMD heterostructures, where the lowest excitation is considered to be the CT exciton [25,26]. On the other hand, the indirect excitation needs to involve a high-order phonon absorption/emission process, whose efficiency can be very low in the optical process. According to our calculation, this excitation comes from the CT exciton. More investigations are needed to further clarify this problem.

Finally, we summarize the several approximations in our study. First, the excimer excitation spectra are calculated from the material parameters constructed from the ML TMDs including experimental measurements [28,35–39] and theoretical calculations [22,23,41]. However, when the sample is synthesized from ML to BL, both the energy bands and the dielectric environment can be influenced [24,28,41]. This may also cause the energy shift for the optical excitation in BL TMDs compared to the ML situation. Nevertheless, this cannot modify the physical picture for the four elementary excitations we reveal here. Second, in our calculation, we only include the bright exciton for the excimer excitation energy. This is because although the dark exciton can also contribute to the formation of the excimer state, on one hand, it has negligible influence on the excimer energy level; on the other hand, it cannot be excited in the optical process. Hence, in the optical process, only the bright exciton is considered.

ACKNOWLEDGMENTS

This work was supported by the National Natural Science Foundation of China under Grant No. 11334014, the National Basic Research Program of China under Grant No. 2012CB922002, and the Strategic Priority Research Program of the Chinese Academy of Sciences under Grant No. XDB01000000.

APPENDIX A: EXCIMER HAMILTONIAN

In this appendix, based on the $\mathbf{k}\cdot\mathbf{p}$ Hamiltonian, we give the explicit form of the excimer Hamiltonian $H^{\mathrm{eh}}_{\substack{m'n'\\mn}}\left(\begin{smallmatrix}\mathbf{r}'_1\mathbf{r}'_2\\ \mathbf{r}_1\mathbf{r}_2\end{smallmatrix}\right)$ for the exciton envelop function $\tilde{F}_{mn}(\mathbf{r}_1,\mathbf{r}_2)$ in the coordinate space, where $m(m')$ and $n(n')$ denote the indices including the layer, valley, and spin degrees of freedom for the electron and hole [33,49,50].

The $\mathbf{k}\cdot\mathbf{p}$ Hamiltonian with the basis $|d^u_{z^2}\rangle$, $|d^l_{z^2}\rangle$, $\frac{1}{\sqrt{2}}(|d^u_{x^2-y^2}\rangle - i\tau_z|d^u_{xy}\rangle)$, and $\frac{1}{\sqrt{2}}(|d^l_{x^2-y^2}\rangle + i\tau_z|d^l_{xy}\rangle)$ reads [22,23]

$$\hat{H} = \begin{pmatrix} \Delta - \tau_z s_z \lambda_c + Ed/2 & 0 & at(\tau_z k_x + ik_y) & 0 \\ 0 & \Delta + \tau_z s_z \lambda_c - Ed/2 & 0 & at(\tau_z k_x - ik_y) \\ at(\tau_z k_x - ik_y) & 0 & -\tau_z s_z \lambda_v + Ed/2 & \tau_\perp \\ 0 & at(\tau_z k_x + ik_y) & \tau_\perp & \tau_z s_z \lambda_v - Ed/2 \end{pmatrix}. \tag{A1}$$

Here, a is the lattice constant and t represents the effective hopping integral; Δ is the band gap; $2\lambda_c$ ($2\lambda_v$) represents the energy splitting for the conduction (valence) bands; $\tau_\perp$ denotes the interlayer hopping for the hole (it vanishes for the electron); $\tau_z = \pm 1$ stands for the valley index with $\tau_z = 1$ (-1) for the K (K′) valley; s_z denotes the Pauli spin matrix; E and d are the magnitude of the electric field and the interlayer distance, respectively.

The eigenequation expressed by the excimer Hamiltonian for the exciton envelop function satisfies

$$\sum_{mn}\int d\mathbf{r}_1 d\mathbf{r}_2 H^{\mathrm{eh}}_{\substack{m'n'\\mn}}\left(\begin{smallmatrix}\mathbf{r}'_1\mathbf{r}'_2\\ \mathbf{r}_1\mathbf{r}_2\end{smallmatrix}\right)\tilde{F}_{mn}(\mathbf{r}_1,\mathbf{r}_2) = E\tilde{F}_{m'n'}(\mathbf{r}'_1,\mathbf{r}'_2), \tag{A2}$$

where

$$\begin{aligned} H^{\mathrm{eh}}_{\substack{m'n'\\mn}}\left(\begin{smallmatrix}\mathbf{r}'_1\mathbf{r}'_2\\ \mathbf{r}_1\mathbf{r}_2\end{smallmatrix}\right) = &\left[H^e_{m'm}(\mathbf{k}_1)\delta_{n'n} + H^h_{n'n}(\mathbf{k}_2)\delta_{m'm} + U^{\mathrm{eh}}(\mathbf{r}_1-\mathbf{r}_2)\delta_{m'm}\delta_{n'n} + T_{\substack{m'n'\\mn}}\right]\delta(\mathbf{r}_1-\mathbf{r}'_1)\delta(\mathbf{r}_2-\mathbf{r}'_2) \\ &+ U^{\mathrm{ex}(1)}_{\substack{m'n'\\mn}}\left(\begin{smallmatrix}\mathbf{r}'_1\mathbf{r}'_2\\ \mathbf{r}_1\mathbf{r}_2\end{smallmatrix}\right) + U^{\mathrm{ex}(2)}_{\substack{m'n'\\mn}}\left(\begin{smallmatrix}\mathbf{r}'_1\mathbf{r}'_2\\ \mathbf{r}_1\mathbf{r}_2\end{smallmatrix}\right). \end{aligned} \tag{A3}$$

Here, $\mathbf{k} = -i\nabla$,

$$U^{\mathrm{eh}}(\mathbf{r}_1-\mathbf{r}_2) = -\frac{e^2}{4\pi\varepsilon_0\kappa_l|\mathbf{r}_1-\mathbf{r}_2|}, \tag{A4}$$

with κ_l being $\kappa_\parallel$ ($\kappa \equiv \sqrt{\kappa_\parallel \kappa_\perp}$) if the electron in the m band and hole in the n band are in the same (different) layer;

$$H^e_{m'm}(\mathbf{k}_1) = E_m(\mathbf{k}_0)\delta_{m'm} + \frac{\hbar^2}{2m_0^2}\sum_{m''}[\mathbf{k}_1\cdot\boldsymbol{\pi}_{m'm''}(\mathbf{k}_0)][\mathbf{k}_1\cdot\boldsymbol{\pi}_{m''m}(\mathbf{k}_0)] \times\left[\frac{1}{E_m(\mathbf{k}_0)-E_{m''}(\mathbf{k}_0)}+\frac{1}{E_{m'}(\mathbf{k}_0)-E_{m''}(\mathbf{k}_0)}\right], \tag{A5}$$

$$H^h_{n'n}(\mathbf{k}_2) = -H^e_{\Theta n\Theta n'}(-\mathbf{k}_2), \tag{A6}$$

and

$$T_{\substack{m'n'\\mn}} = T_{n'n}\delta_{m'm} \tag{A7}$$

(with $T_{n'n}$ being nonzero $\tau_\perp$) only when the holes in the n and n' bands are located in the different layers with the same valley and spin degrees of freedom. In Eq. (A5), $\boldsymbol{\pi} = \mathbf{p} + \frac{\hbar}{4m_0^2c^2}[\boldsymbol{\sigma}\times(\nabla V_0)]$ with V_0 denoting the lattice potential. $\boldsymbol{\pi}_{\eta\eta'}(\mathbf{k}_0)$ stands for the matrix elements of $\boldsymbol{\pi}$ between two Bloch wave functions with indices η and η'. The nonzero expressions of $\boldsymbol{\pi}_{\eta\eta'}(\mathbf{k}_0)$ can be obtained from the Hamiltonian Eq. (A1). For the K ($\tau_z = 1$) and K′ ($\tau_z = -1$) valleys,

$$\begin{aligned}
&\langle\uparrow^u_c|\pi_x|\uparrow^u_v\rangle = \langle\downarrow^u_c|\pi_x|\downarrow^u_v\rangle = \tau_z m_0 a t/\hbar,\\
&\langle\uparrow^u_c|\pi_y|\uparrow^u_v\rangle = \langle\downarrow^u_c|\pi_y|\downarrow^u_v\rangle = i m_0 a t/\hbar,\\
&\langle\uparrow^l_c|\pi_x|\uparrow^l_v\rangle = \langle\downarrow^l_c|\pi_x|\downarrow^l_v\rangle = \tau_z m_0 a t/\hbar,\\
&\langle\uparrow^l_c|\pi_y|\uparrow^l_v\rangle = \langle\downarrow^l_c|\pi_y|\downarrow^l_v\rangle = -i m_0 a t/\hbar.
\end{aligned} \tag{A8}$$

We then express the e-h exchange interaction. For $U^{\mathrm{ex}(1)}_{\substack{m'n'\\mn}}(^{\mathbf{r}'_1\mathbf{r}'_2}_{\mathbf{r}_1\mathbf{r}_2})$, it describes that the e-h pair in one IL exciton can virtually recombine and then generate another IL exciton due to the Coulomb interaction directly. We express the e-h exchange interaction Hamiltonian for both the L-R and S-R parts:

$$U^{\mathrm{ex}(1)}_{\substack{m'n'\\mn}}\begin{pmatrix}\mathbf{r}'_1\mathbf{r}'_2\\ \mathbf{r}_1\mathbf{r}_2\end{pmatrix} = H^{\mathrm{LR}}_{\substack{m'n'\\mn}}\begin{pmatrix}\mathbf{r}'_1\mathbf{r}'_2\\ \mathbf{r}_1\mathbf{r}_2\end{pmatrix} + H^{\mathrm{SR}}_{\substack{m'n'\\mn}}\begin{pmatrix}\mathbf{r}'_1\mathbf{r}'_2\\ \mathbf{r}_1\mathbf{r}_2\end{pmatrix}. \tag{A9}$$

For the L-R part,

$$H^{\mathrm{LR}}_{\substack{m'n'\\mn}}\begin{pmatrix}\mathbf{r}'_1\mathbf{r}'_2\\ \mathbf{r}_1\mathbf{r}_2\end{pmatrix} = -\sum_{\alpha\beta}\frac{\hbar^2}{2m_0^2}\pi^\alpha_{\Theta nm}(\mathbf{k}_0)\pi^\beta_{m'\Theta n'}(\mathbf{k}'_0) \times\left\{\frac{1}{[E_m(\mathbf{k}_0)-E_n(\mathbf{k}_0)]^2}+\frac{1}{[E_{m'}(\mathbf{k}'_0)-E_{n'}(\mathbf{k}'_0)]^2}\right\} \times\frac{\partial^2}{\partial\mathbf{r}^\alpha_1\partial\mathbf{r}^\beta_1}U(\mathbf{r}_1-\mathbf{r}'_2)\delta(\mathbf{r}_1-\mathbf{r}_2)\delta(\mathbf{r}'_1-\mathbf{r}'_2), \tag{A10}$$

with α (β) denoting x or y. For the S-R part,

$$H^{\mathrm{SR}}_{\substack{m'n'\\mn}}\begin{pmatrix}\mathbf{r}'_1\mathbf{r}'_2\\ \mathbf{r}_1\mathbf{r}_2\end{pmatrix} = SU_{\substack{m'\Theta n\\ \Theta n'm}}\delta(\mathbf{r}_1-\mathbf{r}_2)\delta(\mathbf{r}_1-\mathbf{r}'_1)\delta(\mathbf{r}_2-\mathbf{r}'_2), \tag{A11}$$

with

$$U_{\substack{m'\Theta n\\ \Theta n'm}} = \frac{1}{S^2}\int d\mathbf{r}_1 d\mathbf{r}_2\left[\Psi^{m'}_{\mathbf{k}'_0}(\mathbf{r}_1)\right]^*\left[\Theta\tilde{\Psi}^n_{\mathbf{k}_0}(\mathbf{r}_2)\right]^* \times U(\mathbf{r}_1-\mathbf{r}_2)\left[\Theta\tilde{\Psi}^{n'}_{\mathbf{k}'_0}(\mathbf{r}_1)\right]\Psi^m_{\mathbf{k}_0}(\mathbf{r}_2). \tag{A12}$$

Here, S is the area of the 2D plane of the BL WS_2.

For $U^{\mathrm{ex}(2)}_{\substack{m'n'\\mn}}(^{\mathbf{r}'_1\mathbf{r}'_2}_{\mathbf{r}_1\mathbf{r}_2})$, it describes that the hole in the CT exciton first hops from one layer to another and then recombines virtually with the electron part to generate the IL exciton due to the Coulomb interaction. The dominant process of this exchange interaction is the L-R part, which is written as

$$\begin{aligned}
&U^{\mathrm{ex}(2)}_{\substack{m'n'\\mn}}\begin{pmatrix}\mathbf{r}'_1\mathbf{r}'_2\\ \mathbf{r}_1\mathbf{r}_2\end{pmatrix}\\
&= -\frac{\hbar^2}{2m_0^2}\sum_{\alpha\beta}\sum_{l''}\frac{\pi^\alpha_{m'\Theta n'}(\mathbf{k}_0)\pi^\beta_{\Theta l''m}(\mathbf{k}'_0)T_{\Theta n\Theta l''}}{[E_m(\mathbf{k}_0)-E_{l''}(\mathbf{k}_0)][E_m(\mathbf{k}_0)-E_n(\mathbf{k}_0)]}\\
&\times\left[\frac{1}{E_m(\mathbf{k}_0)-E_{l''}(\mathbf{k}_0)}+\frac{1}{E_m(\mathbf{k}_0)-E_n(\mathbf{k}_0)}\right]\\
&\times\frac{\partial^2}{\partial\mathbf{r}^\alpha_1\partial\mathbf{r}^\beta_1}U(\mathbf{r}_1-\mathbf{r}'_2)\delta(\mathbf{r}_1-\mathbf{r}_2)\delta(\mathbf{r}'_1-\mathbf{r}'_2).
\end{aligned} \tag{A13}$$

APPENDIX B: DERIVATION OF THE STEADY-STATE DENSITY MATRIX $\rho_s(\mathbf{P})$

In this appendix, we derive the steady-state density matrix $\rho_s(\mathbf{P})$ based on the KSBEs [Eq. (18)]. Generally, the system can be initialized by the elliptically polarized light with the polarization being $x = [I(\sigma_+) - I(\sigma_-)]/[I(\sigma_+) + I(\sigma_-)]$ which varies from -100% to 100%. Accordingly, the pumped electron density associated with the σ_+ (σ_-) light is $n_{\mathrm{ex}}(1+x)/2$ [$n_{\mathrm{ex}}(1-x)/2$] and hence from Eqs. (23) and (24), the initial density matrix for the system can be written as

$$\rho_i(\mathbf{P}) = \frac{a(\mathbf{P})}{4}\begin{pmatrix}1+x & 0 & 0 & 0\\ 0 & 1-x & 0 & 0\\ 0 & 0 & 1-x & 0\\ 0 & 0 & 0 & 1+x\end{pmatrix}, \tag{B1}$$

with

$$a(\mathbf{P}) = \frac{\exp\{-[\varepsilon(\mathbf{P})-\varepsilon_{\mathrm{pump}}]^2/(2\Gamma^2)\}}{\sum_{\mathbf{P}}\exp\{-[\varepsilon(\mathbf{P})-\varepsilon_{\mathrm{pump}}]^2/(2\Gamma^2)\}}. \tag{B2}$$

In the following, we demonstrate that with this initial condition [Eq. (B1)], the system evolves into the steady state with residual polarization $P(t) = x/2$, and the corresponding steady-state density matrix $\rho_s(\mathbf{P})$ is presented.

The exchange interaction Hamiltonian can be split into the off-block-diagonal $[H^{(1)}_{\mathrm{ex}}(\mathbf{P})]$ and block-diagonal $[H^{(2)}_{\mathrm{ex}}(\mathbf{P})]$ [63] parts

$$H_{\mathrm{ex}}(\mathbf{P}) = H^{(1)}_{\mathrm{ex}}(\mathbf{P}) + H^{(2)}_{\mathrm{ex}}(\mathbf{P}), \tag{B3}$$

with

$$H^{(1)}_{\mathrm{ex}}(\mathbf{P}) = \begin{pmatrix}0 & P_+^2 & -P_+^2 & 0\\ P_-^2 & 0 & 0 & -P_-^2\\ -P_-^2 & 0 & 0 & P_-^2\\ 0 & -P_+^2 & P_+^2 & 0\end{pmatrix} \tag{B4}$$

and

$$H_{\rm ex}^{(2)}(\mathbf{P}) = \begin{pmatrix} |\mathbf{P}|^2 & 0 & 0 & -|\mathbf{P}|^2 \\ 0 & |\mathbf{P}|^2 & -|\mathbf{P}|^2 & 0 \\ 0 & -|\mathbf{P}|^2 & |\mathbf{P}|^2 & 0 \\ -|\mathbf{P}|^2 & 0 & 0 & |\mathbf{P}|^2 \end{pmatrix}. \quad \text{(B5)}$$

It can be shown that the block-diagonal part $[H_{\rm ex}^{(2)}(\mathbf{P})]$ in the exchange interaction Hamiltonian [Eq. (17)] has no effect on the PL depolarization dynamics. From the KSBEs [Eq. (18)], the depolarization dynamics for $P_0(\mathbf{P},t) = \mathrm{Tr}[\rho(\mathbf{P},t)I']$ can be written as

$$\partial_t \mathrm{Tr}[\rho(\mathbf{P},t)I'] + i\mathrm{Tr}[H_{\rm ex}(\mathbf{P})\rho(\mathbf{P},t)I']/\hbar - i\mathrm{Tr}[\rho(\mathbf{P},t)H_{\rm ex}(\mathbf{P})I']/\hbar = 0. \quad \text{(B6)}$$

Therefore, from Eq. (B6), with $H_{\rm ex}^{(2)}(\mathbf{P})I' = I'H_{\rm ex}^{(2)}(\mathbf{P})$, $\mathrm{Tr}[H_{\rm ex}^{(2)}(\mathbf{P})\rho(\mathbf{P},t)I'] = \mathrm{Tr}[\rho(\mathbf{P},t)H_{\rm ex}^{(2)}(\mathbf{P})I']$ and hence $H_{\rm ex}^{(2)}(\mathbf{P})$ has no effect on the PL depolarization dynamics.

Accordingly, with the off-block-diagonal part $[H_{\rm ex}^{(1)}(\mathbf{P})]$ of the exchange interaction Hamiltonian, for the system in the steady state, the condition $[H_{\rm ex}^{(1)}(\mathbf{P}),\rho(\mathbf{P},t)] = 0$ for any $\mathbf{P}$ is satisfied. Hence, for the density matrix

$$\rho(\mathbf{P},t) = \begin{pmatrix} \rho_{11}(\mathbf{P},t) & \rho_{12}(\mathbf{P},t) & \rho_{13}(\mathbf{P},t) & \rho_{14}(\mathbf{P},t) \\ & \rho_{22}(\mathbf{P},t) & \rho_{23}(\mathbf{P},t) & \rho_{24}(\mathbf{P},t) \\ & & \rho_{33}(\mathbf{P},t) & \rho_{34}(\mathbf{P},t) \\ & & & \rho_{44}(\mathbf{P},t) \end{pmatrix}, \quad \text{(B7)}$$

it can be proved that

$$\begin{cases} \rho_{11}(\mathbf{P},t) = \rho_{44}(\mathbf{P},t), \\ \rho_{22}(\mathbf{P},t) = \rho_{33}(\mathbf{P},t), \\ \rho_{11}(\mathbf{P},t) - \rho_{22}(\mathbf{P},t) = \rho_{14}(\mathbf{P},t) - \rho_{23}(\mathbf{P},t), \\ \rho_{14}^*(\mathbf{P},t) = \rho_{14}(\mathbf{P},t), \\ \rho_{23}^*(\mathbf{P},t) = \rho_{23}(\mathbf{P},t), \end{cases} \quad \text{(B8)}$$

and the other matrix elements are zero.

Then with the conditions [Eq. (B8)], in order to obtain the exact values of the nonzero terms in the density matrix Eq. (B7), we can derive the relations between these terms based on the dynamical evolution of the density matrix with the initial condition Eq. (B1). The dynamical evolution of the density matrix without the scattering can be obtained with the Baker-Hausdorff formula, which reads

$$\begin{aligned} \rho(\mathbf{P},t) &= \exp\left[iH_{\rm ex}^{(1)}(\mathbf{P})t\right]\rho_i(\mathbf{P})\exp\left[-iH_{\rm ex}^{(1)}(\mathbf{P})t\right] \\ &= \rho_i(\mathbf{P}) + it\left[H_{\rm ex}^{(1)}(\mathbf{P}),\rho_i(\mathbf{P})\right] \\ &\quad + \frac{i^2t^2}{2!}\left[H_{\rm ex}^{(1)}(\mathbf{P}),\left[H_{\rm ex}^{(1)}(\mathbf{P}),\rho_i(\mathbf{P})\right]\right] + \cdots \\ &\quad + \frac{i^nt^n}{n!}H_{\rm com}^{(n)}(\mathbf{P}) + \cdots, \end{aligned} \quad \text{(B9)}$$

with

$$H_{\rm com}^{(n)}(\mathbf{P}) = \Big[\underbrace{H_{\rm ex}^{(1)}(\mathbf{P}),\left[H_{\rm ex}^{(1)}(\mathbf{P}),\cdots\left[H_{\rm ex}^{(1)}(\mathbf{P})}_{n},\rho_i(\mathbf{P})\right]\right]\Big] \quad \text{(B10)}$$

for $n = 1,2,3\cdots$.

It can be calculated that

$$H_{\rm com}^{(2n-1)}(\mathbf{P}) = \frac{1}{2}(16|\mathbf{P}|^4)^{n-1}xa(\mathbf{P}) \times \begin{pmatrix} 0 & -P_+^2 & P_+^2 & 0 \\ P_-^2 & 0 & 0 & -P_-^2 \\ -P_-^2 & 0 & 0 & P_-^2 \\ 0 & P_+^2 & -P_+^2 & 0 \end{pmatrix} \quad \text{(B11)}$$

and

$$H_{\rm com}^{(2n)}(\mathbf{P}) = 2(16|\mathbf{P}|^4)^{n-1}xa(\mathbf{P}) \times \begin{pmatrix} |\mathbf{P}|^4 & 0 & 0 & -|\mathbf{P}|^4 \\ 0 & -|\mathbf{P}|^4 & |\mathbf{P}|^4 & 0 \\ 0 & |\mathbf{P}|^4 & -|\mathbf{P}|^4 & 0 \\ -|\mathbf{P}|^4 & 0 & 0 & |\mathbf{P}|^4 \end{pmatrix}. \quad \text{(B12)}$$

From Eq. (B12), one concludes that

$$\begin{cases} \rho_{11}(\mathbf{P},t) + \rho_{14}(\mathbf{P},t) = a(\mathbf{P})(1+x)/4, \\ \rho_{22}(\mathbf{P},t) - \rho_{14}(\mathbf{P},t) = a(\mathbf{P})(1-x)/4, \\ \rho_{14}(\mathbf{P},t) = -\rho_{23}(\mathbf{P},t). \end{cases} \quad \text{(B13)}$$

From Eqs. (B8) and (B13), when the system is in the steady state, we obtain

$$\rho_s(\mathbf{P}) = \frac{a(\mathbf{P})}{4}\begin{pmatrix} 1+x/2 & 0 & 0 & x/2 \\ 0 & 1-x/2 & -x/2 & 0 \\ 0 & -x/2 & 1-x/2 & 0 \\ x/2 & 0 & 0 & 1+x/2 \end{pmatrix}. \quad \text{(B14)}$$

Therefore, from Eq. (21), the steady-state PL polarization is calculated to be $P(t) = x/2$, which is half of the polarization of the elliptically polarized light. Specifically, with the system pumped by the σ_+ (σ_-) light, $x = 100\%$ ($x = -100\%$) and hence the steady-state PL polarization is $P(t) = 50\%$ [$P(t) = -50\%$] exactly.

[1] K. F. Mak, C. G. Lee, J. Hone, J. Shan, and T. F. Heinz, Phys. Rev. Lett. **105**, 136805 (2010).

[2] A. Splendiani, L. Sun, Y. B. Zhang, T. S. Li, J. Kim, C. Y. Chim, G. Galli, and F. Wang, Nano Lett. **10**, 1271 (2010).

[3] Z. Y. Zhu, Y. C. Cheng, and U. Schwingenschlögl, Phys. Rev. B **84**, 153402 (2011).

[4] T. Cao, G. Wang, W. Han, H. Ye, C. Zhu, J. Shi, Q. Niu, P. Tan, E. Wang, B. Liu, and J. Feng, Nat. Commun. **3**, 887 (2012).

[5] D. Xiao, G. B. Liu, W. Feng, X. Xu, and W. Yao, Phys. Rev. Lett. **108**, 196802 (2012).

[6] G. Sallen, L. Bouet, X. Marie, G. Wang, C. R. Zhu, W. P. Han, Y. Lu, P. H. Tan, T. Amand, B. L. Liu, and B. Urbaszek, Phys. Rev. B **86**, 081301(R) (2012).

[7] K. Kaasbjerg, K. S. Thygesen, and K. W. Jacobsen, Phys. Rev. B **85**, 115317 (2012).

[8] T. Cheiwchanchamnangij and W. R. L. Lambrecht, Phys. Rev. B **85**, 205302 (2012).

[9] E. S. Kadantsev and P. Hawrylak, Solid State Commun. **152**, 909 (2012).

[10] K. F. Mak, K. He, J. Sahn, and T. F. Heinz, Nat. Nanotechnol. **7**, 494 (2012).

[11] G. Kioseoglou, A. T. Hanbicki, M. Currie, A. L. Friedman, D. Gunlycke, and B. T. Jonker, Appl. Phys. Lett. **101**, 221907 (2012).

[12] H. Zeng, J. Dai, W. Yao, D. Xiao, and X. Cui, Nat. Nanotechnol. **7**, 490 (2012).

[13] H. Shi, H. Pan, Y. W. Zhang, and B. I. Yakobson, Phys. Rev. B **87**, 155304 (2013).

[14] X. Li, J. T. Mullen, Z. Jin, K. M. Borysenko, M. Buongiorno Nardelli, and K. W. Kim, Phys. Rev. B **87**, 115418 (2013).

[15] K. Kośmider and J. Fernández-Rossier, Phys. Rev. B **87**, 075451 (2013).

[16] H. Ochoa and R. Roldán, Phys. Rev. B **87**, 245421 (2013).

[17] F. Zahid, L. Liu, Y. Zhu, J. Wang, and H. Guo, AIP Adv. **3**, 052111 (2013).

[18] L. Wang and M. W. Wu, Phys. Lett. A **378**, 1336 (2014); Phys. Rev. B **89**, 115302 (2014); **89**, 205401 (2014).

[19] D. Lagarde, L. Bouet, X. Marie, C. R. Zhu, B. L. Liu, T. Amand, P. H. Tan, and B. Urbaszek, Phys. Rev. Lett. **112**, 047401 (2014).

[20] S. F. Wu, J. S. Ross, G. B. Liu, G. Aivazian, A. Jones, Z. Y. Fei, W. G. Zhu, D. Xiao, W. Yao, D. Cobden, and X. D. Xu, Nat. Phys. **9**, 149 (2013).

[21] H. T. Yuan, M. S. Bahramy, K. Morimoto, S. F. Wu, K. Nomura, B. J. Yang, H. Shimotani, R. Suzuki, M. Toh, C. Kloc, X. D. Xu, R. Arita, N. Nagaosa, and Y. Iwasa, Nat. Phys. **9**, 563 (2013).

[22] Z. Gong, G. B. Liu, H. Yu, D. Xiao, X. D. Cui, X. D. Xu, and W. Yao, Nat. Commun. **4**, 2053 (2013).

[23] A. M. Jones, H. Yu, J. S. Ross, P. Klement, N. J. Ghimire, J. Q. Yan, D. G. Mandrus, W. Yao, and X. D. Xu, Nat. Phys. **10**, 130 (2014).

[24] W. J. Zhao, R. M. Ribeiro, M. L. Toh, A. Carvalho, C. Kloc, A. H. C. Neto, and G. Eda, Nano Lett. **13**, 5627 (2013).

[25] P. Rivera, J. R. Schaibley, A. M. Jones, J. S. Ross, S. Wu, G. Aivazian, P. Klement, N. J. Ghimire, J. Yan, D. G. Mandrus, W. Yao, and X. D. Xu, arXiv:1403.4985.

[26] Y. F. Yu, S. Hu, L. Q. Su, L. J. Huang, Y. Liu, Z. H. Jin, A. A. Purezky, D. B. Geohegan, K. W. Kim, Y. Zhang, and L. Y. Cao, arXiv:1403.6181.

[27] B. R. Zhu, H. L. Zeng, J. F. Dai, Z. R. Gong, and X. D. Cui, arXiv:1403.6224.

[28] B. Zhu, X. Chen, and X. D. Cui, arXiv:1403.5108.

[29] I. Michl and V. Bonacic-Koutecky, *Electronic Aspects of Organic Photochemistry* (Wiley, New York, 1990).

[30] M. W. Wu and E. M. Conwell, Phys. Rev. B **56**, R10060(R) (1997).

[31] T. Yu and M. W. Wu, Phys. Rev. B **89**, 205303 (2014).

[32] M. M. Glazov, T. Amand, X. Marie, D. Lagarde, L. Bouet, and B. Urbaszek, Phys. Rev. B **89**, 201302 (2014).

[33] M. Z. Maialle, E. A. de Andrada e Silva, and L. J. Sham, Phys. Rev. B **47**, 15776 (1993).

[34] A. Vinattieri, Jagdeep Shah, T. C. Damen, D. S. Kim, L. N. Pfeiffer, M. Z. Maialle, and L. J. Sham, Phys. Rev. B **50**, 10868 (1994).

[35] A. R. Klots, A. K. M. Newaz, Bin Wang, D. Prasai, H. Krzyzanowska, D. Caudel, N. J. Ghimire, J. Yan, B. L. Ivanov, K. A. Velizhanin, A. Burger, D. G. Mandrus, N. H. Tolk, S. T. Pantelides, and K. I. Bolotin, arXiv:1403.6455.

[36] A. Chernikov, T. C. Berkelbach, H. M. Hill, A. Rigosi, Y. Li, O. B. Aslan, D. R. Reichman, M. S. Hybertsen, and T. F. Heinz, arXiv:1403.4270.

[37] Z. Ye, T. Cao, K. O'Brien, H. Zhu, X. Yin, Y. Wang, S. G. Louie, and X. Zhang, arXiv:1403.5568.

[38] M. M. Ugeda, A. J. Bradley, S. F. Shi, F. H. da Jornada, Y. Zhang, D. Y. Qiu, S. K. Mo, Z. Hussain, Z. X. Shen, F. Wang, S. G. Louie, and M. F. Crommie, arXiv:1404.2331.

[39] G. Wang, X. Marie, I. Gerber, T. Amand, D. Lagarde, L. Bouet, M. Vidal, A. Balocchi, and B. Urbaszek, arXiv:1404.0056.

[40] A. Ramasubramaniam, Phys. Rev. B **86**, 115409 (2012).

[41] A. Kumar and P. K. Ahluwalia, Phys. B **407**, 4627 (2012).

[42] C. Ataca, M. Topsakal, E. Aktürk, and S. Ciraci, J. Phys. Chem. C **115**, 16354 (2011).

[43] M. W. Wu and H. Metiu, Phys. Rev. B **61**, 2945 (2000).

[44] M. W. Wu, J. H. Jiang, and M. Q. Weng, Phys. Rep. **493**, 61 (2010).

[45] G. Plechinger, P. Nagler, C. Schüller, and T. Korn, arXiv:1404.7674.

[46] C. Mai, A. Barrette, Y. Yu, Y. G. Semenov, K. W. Kim, L. Cao, and K. Gundogdu, Nano Lett. **14**, 202 (2014).

[47] Q. Wang, S. Ge, X. Li, J. Qiu, Y. Ji, J. Feng, and D. Sun, ACS Nano **7**, 11087 (2013).

[48] T. Korn, S. Heydrich, M. Hirmer, J. Schmutzler, and C. Schüller, Appl. Phys. Lett. **99**, 102109 (2011).

[49] G. E. Pikus and G. L. Bir, Zh. Eksp. Teor. Fiz. **60**, 195 (1971) [Sov. Phys. JETP **33**, 108 (1973)].

[50] H. Tong and M. W. Wu, Phys. Rev. B **83**, 235323 (2011).

[51] L. Hromadová, R. Martoňák, and E. Tosatti, Phys. Rev. B **87**, 144105 (2013).

[52] *Semiconductors. Physics of Group IV Elements and III-V Compounds*, edited by O. Madelung, M. Schultz, and H. Weiss, Landolt-Börnstein, New Series, Group III, Vol. 17, Pt. A (Springer-Verlag, Berlin, 1982).

[53] H. Haug and A.-P. Jauho, *Quantum Kinetics in Transport and Optics of Semiconductors* (Springer-Verlag, Berlin, 1996).

[54] S. Tongay, J. Zhou, C. Ataca, J. Liu, J. S. Kang, T. S. Matthews, L. You, J. Li, J. C. Grossman, and J. Wu, Nano Lett. **13**, 2831 (2013).

[55] T. Ando, A. B. Fowler, and F. Stern, Rev. Mod. Phys. **54**, 437 (1982).

[56] *Optical Orientation, Modern Problems in Condensed Matter Science*, edited by F. Meier and B. P. Zakharchenya (North-Holland, Amsterdam, 1984), Vol. 8.

[57] *Semiconductor Spintronics and Quantum Computation*, edited by D. D. Awschalom, D. Loss, and N. Samarth (Springer, Berlin, 2002).

[58] I. Žutić, J. Fabian, and S. D. Sarma, Rev. Mod. Phys. **76**, 323 (2004).

[59] J. Fabian, A. Matos-Abiague, C. Ertler, P. Stano, and I. Žutić, Acta Phys. Slov. **57**, 565 (2007).

[60] *Spin Physics in Semiconductors*, edited by M. I. D'yakonov (Springer, New York, 2008).

[61] T. Korn, Phys. Rep. **494**, 415 (2010).

[62] *Handbook of Spin Transport and Magnetism*, edited by E. Y. Tsymbal and I. Žutić (CRC Press, Boca Raton, FL, 2011).

[63] This can be seen clearly by adjusting the order of the basis of $H_{\rm ex}(\mathbf{P})$.